A MCC950 analogue inflammasome inhibitor reduces the foreign body reaction against neural implants

European Journal of Medicinal Chemistry Reports 17 (2026) 100357

Contents lists available at ScienceDirect

European Journal of Medicinal Chemistry Reports

journal homepage: www.editorialmanager.com/ejmcr/default.aspx

A MCC950 analogue inflammasome inhibitor reduces the foreign body reaction against neural implants

Jose Crugeiras [a,d,1], Chiara Bisquoli [b,1], María Rodríguez-Brañas [a], Bruno Rodríguez-Meana [a,d], Tiziano De Ventura [b], Neus Hernández [a,d], Jessica Jaramillo [a,d], Alice Honovich [b], Ignacio Delgado-Martínez [a,e], Natalia Lago [a,d], Hanna Karlsson-Fernberg [f], Maria Asplund [f], Stefano Carli [c], Claudio Trapella [b], Giulia Turrin [c,*], Xavier Navarro [a,d,**]

[a] Institute of Neurosciences, Department of Cell Biology, Physiology and Immunology, Universitat Autònoma de Barcelona, Campus UAB, Bellaterra, 08193, Spain
[b] Department of Chemical, Pharmaceutical and Agricultural Sciences, University of Ferrara, Via Fossato di Mortara 17-19, Ferrara, 44121, Italy
[c] Department of Environmental and Prevention Sciences, University of Ferrara, Via Luigi Borsari 46, Ferrara, 44141, Italy
[d] Centro de Investigación Biomédica en Red en Enfermedades Neurodegenerativas (CIBERNED), Monforte de Lemos 3-5, Madrid, 28029, Spain
[e] Department of Morphological Sciences, Universitat Autònoma de Barcelona, Campus UAB, Bellaterra, 08193, Spain
[f] Department of Microtechnology and Nanoscience, Chalmers University of Technology, Kemivägen 9, Gothenburg, 412 58, Sweden

ARTICLE INFO

Keywords:
Foreign body reaction
Inflammasome
Intraneural electrode
Macrophages
Neuroprosthesis
Sulfonamide
MCC950

ABSTRACT

Devices implanted in the body provoke a foreign body reaction (FBR) that results in tissue encapsulation of the device and hampers its functionality over time. This FBR is particularly relevant regarding long-term implanted neural electrodes. Inflammasome inhibitors may represent a novel treatment to reduce the initial macrophage activation, and thus reduce the FBR and improve the outcome of implanted devices. We have synthetized an inflammasome inhibitor, named TDV19, and tested its capability to reduce macrophage activation in vitro, in comparison with the standard inhibitor MCC950. Then, polyimide thin-film devices were longitudinally implanted in the rat sciatic nerve and tested for 2 months to evaluate the intraneural FBR. Systemic administration of TDV19 and of MCC950 significantly reduced macrophage infiltration in the nerve and thickness of the fibrotic capsule around the device. Thus, systemic administration of inflammasome inhibitors appears as a useful treatment to improve the fate of chronically implanted neural electrodes.

1. Introduction

Neuroprostheses are devices that help restoring sensorimotor functions lost or impaired due to neural injuries, limb amputation or congenital conditions. Achieving this goal requires electrodes capable of establishing bidirectional communication between the nervous system and the external prosthesis. For this purpose, the electrodes must connect with specific neural pathways, both motor and sensory, enabling stable, long-term biocompatible integration [1,2]. However, the implantation of any device in the body triggers activation of the innate immune system, in order to eliminate the foreign material and restore homeostasis. This response, known as the Foreign Body Reaction (FBR), interferes with normal wound-healing processes by altering molecular cascades involved in tissue repair. The FBR can be divided into three stages: i) protein adsorption on the implant surface, ii) inflammation, and iii) fibrosis. In the initial stage, plasma proteins such as albumin, fibronectin, fibrinogen, vitronectin, or γ-globulin adsorb onto the implant surface [3–5], contributing to the formation of a provisional extracellular matrix (ECM). Subsequently, mast cells and neutrophils infiltrate the tissue, after which macrophages are recruited and transition through a pro-inflammatory phase—characterized by secretion of pro-inflammatory cytokines—followed by an anti-inflammatory phase. In later stages, fibroblasts, activated in part by macrophage-derived cytokines, produce collagen and establish a definitive matrix, ultimately leading to the formation of a fibrotic capsule surrounding the implant [3,4,6]. This capsule may compromise the durability, viability,

* Corresponding author.
** Corresponding author. Institute of Neurosciences, Department of Cell Biology, Physiology and Immunology, Universitat Autònoma de Barcelona, Campus UAB, 08193, Bellaterra, Spain.
E-mail addresses: giulia.turrin@unife.it (G. Turrin), xavier.navarro@uab.cat (X. Navarro).
[1] These authors contributed equally as first authors to this work.

https://doi.org/10.1016/j.ejmcr.2026.100357
Received 16 February 2026; Received in revised form 30 June 2026; Accepted 3 July 2026
Available online 10 July 2026

and functionality of the implant; in the case of electrodes implanted in peripheral nerves, it is associated with increased impedance, higher current requirements for axonal stimulation, and reduced ability to record electrical signals [7–10]. In order to improve biocompatibility and extend implant functionality, various strategies have been investigated to mitigate the FBR. Among them, local or systemic administration of anti-inflammatory or antifibrotic agents, such as dexamethasone or metformin, has been explored [11,12]. However, these approaches often face limitations, including systemic toxicity or side effects, transient efficacy, or challenges in achieving localized delivery.

In FBR models not directly related to the nervous system, NLRP3 inflammasome inhibitors have been proposed as potential candidates for reducing fibrosis [13]. Inflammasomes are a heterogeneous family of multiprotein complexes that share the ability to become activated in response to stressors, thereby maintaining homeostasis and responding to physiological aberrations [14]. Upon exposure to endogenous (DAMPs) or exogenous (PAMPs) danger signals, such as bacterial infections or tissue damage induced during surgery [15,16], inflammasome proteins assemble and promote activation of the proteolytic enzyme caspase-1. This enzyme mediates the proteolytic processing of pro-IL-1β and pro-IL-18 into their active forms, which are responsible for driving the inflammatory response. Hence, inhibiting the assembly of NLRP3 inflammasome has emerged as a promising therapeutic strategy for inflammation-related disease. Since NLRP3 acts upstream of IL-1β and IL-18, it represents an attractive target to attenuate pathological inflammation without broadly compromising immune function. MCC950 (also known as CP-456,773) is a diaryl-sulfonylurea derivative, firstly identified as an antagonist of IL-1β and classified as a cytokine release antagonist [16]. Further studies revealed that MCC950 reduces the maturation and release of IL-1β by inhibiting activation of the NLRP3 inflammasome [17,18]. Thus, MCC950 is currently considered a specific small-molecule inhibitor that selectively blocks activation of the NLRP3 inflammasome, by blocking NLRP3 oligomerization mediated by the ASC adaptor protein, a critical step in inflammasome assembly and activation [18].

In the context of the FBR onset, the NLRP3 inflammasome may play a pivotal role in sustaining chronic inflammation, since local inhibition of this receptor using MCC950 markedly reduced FBR generation [19,20]. The first aim of this work was to synthesize a synthetic analogue, termed TDV19 (see patent WO2024/010,772-A1), that would preserve the biological activity of MCC950, but at the same time would have higher chemical reactivity in anchoring to a solid surface, such as a neural implant or other device, in order to minimize the onset of FBR, and would avoid potential side effects.

The chemical structure of TDV19 differs slightly from that of MCC950. The diaryl-sulfonylurea scaffold was selected as the pharmacophore, together with the tricyclic indacenamine moiety, which is essential for biological activity. The tricyclic core is a structural motif frequently found in several pharmaceutical compounds with antiproliferative [21] and antimicrobial [22] activity. The main chemical modification realized involves the alcohol functionality at position 3 of the furan heterocyclic ring. The rationale for replacing the tertiary alcohol with a more reactive and less sterically hindered primary hydroxyl group lies in the possibility of exploiting this functional group to attach TDV19 onto the polymer surface of implantable electrodes. To better evaluate its activity on the foreign body response (FBR) prior to electrode anchoring, we synthesized the analogue TDV19. Then, we evaluated the efficacy of TDV19 to modulate the macrophage inflammatory response in comparison with MCC950, and assessed whether its administration attenuates the in vivo FBR against intraneural implants.

2. Material and methods

2.1. Synthetic procedures

All chemicals and solvents were purchased by Merk and Carlo Erba Reagents, respectively, except otherwise specified. Reaction progress and product mixtures were monitored by thin-layer chromatography (TLC) on silica gel (precoated F254 Macherey-Nagel plates) and visualized with a UV lamp (254 nm light source). The organic solutions from extractions were dried over anhydrous sodium sulfate. Flash column chromatography was undertaken on silica gel Merck 60–200 mesh using chromatography (Isolera, Biotage, Sweden). ^{1}H, ^{13}C, DEPT, NMR spectra were recorded on a VARIAN Mercury Plus 400 MHz spectrometer. Chemical shifts (δ) are reported in parts per million (ppm) using the peak of deuterated solvents as an internal standard and coupling constants (J) are reported in Hertz. Splitting patterns are designed as follows: s, singlet; d, doublet; t, triplet; q, quartet; m, multiplet; b, broad. Melting points for purified products were determined in a glass capillary on a Stuart Scientific electrothermal apparatus SMP3 and are uncorrected. Molecular weights were measured with a mass spectrometer ESI MICROMASS ZMD 2000 (Waters, Manchester, UK) and high-resolution spectra with an Agilent ESI-Q- TOF LC/MS 6520 system (Agilent Technologies, USA.). Analytical control of the final product was performed using Agilent 1260 Infinity II analytical HPLC using a Luna® C18 column (150 × 4.6 mm, 5 μm). The products were analyzed using a binary eluent system consisting of ACN (solution B) and H_2O (solution A), both acidified with 0.1% v/v HCOOH, at a flow rate of 0.5 mL/min, temperature of the column 40°C.

The purity of all compounds was determined by HPLC and was greater than 95%. ATR-FTIR spectra were collected with a Nicolet iS50 spectrometer (Thermo Fisher Scientific) with a Diamond-ATR element fixed at a 45° incident angle. Uv-vis spectra were taken in transmission mode with an Agilent Carry 300 UV-Vis spectrophotometer.

2.1.1. Synthesis of ethyl 5-(chlorosulfonyl)furan-3-carboxylate (3)

Ethyl-3-furoate (**2**) (2.9 g, 20.7 mmol) was dissolved in anhydrous DCM (40 mL) under nitrogen atmosphere and cooled to −10°C. Chlorosulfonic acid (1.5 mL, 22.05 mmol) was added to the cooled solution dropwise over 10 min. After addition, the reaction was allowed to warm to room temperature and stirred for 72h to give a green solution with white slurry. The mixture was cooled to −10°C and anhydrous pyridine (1.8 mL, 22.89 mmol) was added dropwise over 10 min. Subsequently, PCl_5 (4.8 g, 22.89 mmol) was added portion wise at −8°C. The reaction was stirred at 0°C for 30 min, then at room temperature overnight. The reaction was quenched with water (60 mL) and then stirred for 45 min after addition. The layers were separated and the organic layers were washed with water (2 × 30 mL). The combined organic extracts were dried with Na_2SO_4, filtered and concentrated in vacuo to give the crude products as a brown oil, ethyl 5-(chlorosulfonyl) furan-3-carboxylate (**3**). Yield: 77%.

^{1}H NMR (400 MHz, Chloroform-d) δ 8.22 (d, J = 0.9 Hz, 1H, O-C*H*=C (furane)), 7.60 (d, J = 0.9 Hz, 1H, C*H*-furane), 4.37 (q, J = 7.1 Hz, 2H, O-C*H*$_2$-CH$_3$), 1.41 – 1.34 (m, 3H, O-CH$_2$-C*H*$_3$).

^{13}C NMR (101 MHz, Chloroform-*d*) δ 160.65, (q, C=O), 151.44 (q, C-S), 150.89, (CH, O-*C*H=C), 121.76, (q, C=*C*-C=O), 118.22, (S-C=*C*-C (Furane C2), 61.85, (O-*C*H$_2$-CH$_3$), 14.35, (O-CH$_2$-*C*H$_3$).

2.1.2. Synthesis of ethyl 5-sulfamoylfuran-3-carboxylate (4)

Compound **3** (1.5 g, 6.3 mmol) was dissolved in acetone (10 mL) at room temperature. Saturated ammonium bicarbonate solution (2 g, 25.2 mmol) was added dropwise at room temperature. The mixture reacted for 3 h at room temperature, monitored by TLC until complete conversion. After an extraction with ethyl acetate (AcOEt, 200 mL × 3), the combined organic phases were dried over anhydrous Na_2SO_4, and the solvent was evaporated. Purification was carried out by silica gel column chromatography with A/P 3:7 v/v to obtain ethyl 5-sulfamoylfuran-3-carboxylate (**4**) as a white crystalline solid. mp: 130-131°C. Yield 53%.

^{1}H NMR (400 MHz, DMSO-d6) δ 8.63 (d, J = 1.0 Hz, 1H, O-C*H*=C (furane)), 7.94 (s, 2H, N*H*$_2$), 7.12 (d, J = 1.0 Hz, 1H, C*H*-furane), 4.27 (q, J = 7.1 Hz, 2H, O-C*H*$_2$-CH$_3$), 1.35 – 1.22 (m, 3H, O-CH$_2$-C*H*$_3$).

^{13}C NMR (101 MHz, DMSO) δ 161.31, (q, C=O), 153.49, (q, C-S), 150.36, (CH, O-*C*H=C), 119.57, (q, C=*C*-C=O), 111.55, (S-C=*C*H-C (Furane C2), 60.74, (O-*C*H_2-CH_3), 14.10, (O-CH_2-*C*H_3).

2.1.3. Synthesis of 4-(hydroxymethyl)furan-2-sulfonamide (5)

Compound **4** (1.35 g, 6.1 mmol) in anhydrous THF (20 mL) was cooled to 0°C. $LiAlH_4$ was added (9.2 mmol) portion wise, then the reaction was heated to 60°C for 2 h. After this time, the reaction was allowed to warm to room temperature and a saturated solution of ammonium chloride (NH_4Cl) was added dropwise to neutralize aluminum salts, and the reaction was stirred for 30 min. Then ethyl ether (Et_2O) was added, and the mixture was stirred for 10 min. Subsequently, AcOEt was added, and the solvent was decanted. This operation was repeated 3 times. The combined organic extracts were dried with Na_2SO_4, filtered and concentrated in vacuo to give 4-(hydroxymethyl) furan-2-sulfonamide (**5**), as a yellowish oil. Yield 87%.

^{1}H NMR (400 MHz, DMSO-d6) δ 7.75 (q, J = 1.0 Hz, 1H, O-C*H*=C (furane)), 7.69 (s, 2H, N*H*$_2$), 6.89 (d, J = 1.0 Hz, 1H, C*H*-furane), 5.13 (s, 1H, CH_2-O*H*), 4.42 – 4.28 (m, 2H, C*H*$_2$-OH).

^{13}C NMR (101 MHz, DMSO) δ 152.44, (q, C-S), 142.49, (CH, O-*C*H=C), 128.12, (q, C=*C*-C=O), 113.40, (S-C=*C*H-C (Furane C2), 54.77, (*C*H_2-OH).

2.1.4. Synthesis of 4-(hydroxymethyl)furan-2-sulfonyl azide (6)

Compound **5** (940 mg, 5.31 mmol) and K_2CO_3 (2.93 g, 21.24 mmol) were dissolved in 60 mL of a mixture of deionized water and isopropyl alcohol (1:1). Then, imidazole-1-sulphonyl azide hydrogen sulfate salt (diazotransfer, 2.15 g, 7.96 mmol) was added, and the mixture was stirred for 18h at room temperature. Then, the reaction was diluted with 60 mL of $NaHCO_{3\ sat.}$ And extracted with AcOEt (3 × 60 mL). Organic phases were combined, washed with Brine (80 mL), dried with Na_2SO_4, filtered and concentrated in vacuo. Purification was carried out by silica gel column chromatography with A/P 1:1 v/v to obtain 4-(hydroxymethyl)furan-2-sulfonyl azide (**6**) as a yellowish crystalline solid. mp: 133-134°C. Yield 58%.

^{1}H NMR (400 MHz, Chloroform-d) δ 7.67 (q, J = 1.0 Hz, 1H, O-C*H*=C (furane)), 7.27 (d, J = 1.0 Hz, 1H, C*H*-furane), 4.64 (d, J = 1.0 Hz, 2H, C*H*$_2$-OH).

^{13}C NMR (101 MHz, cdcl3) δ 146.93, (q, C-S), 145.01, (CH, O-*C*H=C), 127.55, (q, C=*C*-C=O), 118.76, (S-C=*C*H-C (Furane C2), 56.04, (*C*H_2-OH).

2.1.5. Synthesis of N-((1,2,3,5,6,7-hexahydro-s-indacen-4-yl)carbamoyl)-4-(hydroxymethyl) furan-2-sulfonamide (1, TDV19)

Compound **6** (138 mg, 0.68 mmol), $Pd(OAc)_2$ (1.5 mg, 0.006 mmol), and 1,2,3,5,6,7-hexahydro-s-indacen-4-amine (117.6 mg, 0.68 mmol) were dissolved in anhydrous ACN (7 mL). The system was then evacuated under vacuum, after which a CO balloon was attached very carefully, ensuring that the system was completely sealed and located under a chemical hood during the reaction and the subsequent treatments. The mixture was stirred overnight.

The crude was diluted with DCM (20 mL), washed with HCl 1M (20 mL) and the aqueous phase was extracted with DCM (3 × 20 mL). The organic layers were combined, dried with Na_2SO_4, filtered and concentrated in vacuo to give compound N-((1,2,3,5,6,7-hexahydro-s-indacen-4-yl)carbamoyl)-4 (hydroxymethyl)furan-2-sulfonamide (**1**), that will be referred to as TDV19 (**1**). The crude was purified performing an Et_2O trituration. mp: 155-156°C. Yield 50%.

^{1}H NMR (400 MHz, DMSO-d6) δ 10.95 (s, 1H, Indacen-N*H*-C=O), 8.11 (s, 1H, SO_2-N*H*-C=O), 7.88 (s, 1H, O-C*H*=C (furane)), 7.18 (s, 1H, C*H*-furane), 6.95 (s, 1H, Indacen-C*H*$_{Aromatic}$), 5.17 (bs, 1H, O*H*), 4.35 (s, 2H, C*H*$_2$-OH), 2.79 (t, J = 7.4 Hz, 4H, C_{Ar}-C*H*$_2$-CH_2-CH_2-C_{Ar}), 2.60 (t, J = 7.4 Hz, 4H, C_{Ar}-CH_2-CH_2-C*H*$_2$-C_{Ar}), 1.95 (p, J = 7.4 Hz, 4H, (C_{Ar}-CH_2-C*H*$_2$-CH_2-C_{Ar}). ^{13}C NMR (101 MHz, DMSO-d_6) δ 148.97, (NH-*C*=O), 148.07, (q, C-S), 144.13, (CH, O-*C*H=C), 143.57, (q C_{Ar}), 137.75, (q C_{Ar}), 128.96, (q C_{Ar}), 128.71, (q C_{Ar}), 118.57, (S-C=*C*H-C (Furane C2), 117.90(CH_{Ar}), 54.72, (*C*H_2-OH), 32.89, (C_{Ar}-*C*H_2-CH_2-CH_2-C_{Ar}), 30.55, (C_{Ar}-CH_2-CH_2-*C*H_2-C_{Ar}), 25.50, (C_{Ar}-CH_2-*C*H_2-CH_2-C_{Ar}).

2.2. In vitro studies of macrophage response

Four-weeks old female Sprague Dawley rats were euthanized with pentobarbital (200 mg/kg i. p.) and cleaned with ethanol 70%. Femur and tibia bones were dissected, bone epiphyses removed, and the bone marrow flushed with DPBS (Gibco, Cat #14190144). The collected extract was centrifuged at 1900 rpm for 10 min and cells were cultured in 100 mL Petri plates with DMEMF/12 medium (Gibco, Cat #31330038) that contained 10% hiFBS (Gibco, Cat#A5256701) and 1X penicillin/streptomycin (Sigma, Cat #P0781). Macrophage colony-stimulating factor (M-CSF) (PrepoTech, Cat #400-28) was added at 10 ng/mL to obtain a culture of bone marrow derived macrophages (BMDM). The culture medium was replaced every three days. At 8 days in vitro, cells were reseeded in 24-well plates at 3.5×10^5 cells/well. At 48h after seeding, macrophages were incubated with MCC950 or TDV19 (both 7.5 nM) for 30 min and then lipopolysaccharide (LPS) was added at 10 μg/mL for 4 h to induce the model of pro-inflammatory macrophages. In an additional comparative experiment, BDMD were treated with LPS (4 h) followed by ATP 5 mM (30 min).

For calculating the IC50 of TDV19, we added the compound at concentrations of 0.1, 0.3, 1, 3, 10, 30, 100, 300 and 1000 nM to the BMDM culture, and assayed the release of IL-1β by ELISA (see below).

Nitric oxide (NO) production by reactive macrophages was assessed in the supernatant through a Griess assay. A volume of 100 μL from each sample was mixed with 100 μL of Griess reagent (Sigma, Cat #G4410) and incubated for 15 min. Absorbance was then recorded at 540 nm using a Varikoskan Lux microplate reader (Thermo Scientific). The nitrite concentration was calculated by subtracting the absorbance of the sample from that of the blank, and the result was interpolated from the $NaNO_2$ standard curve (Sigma, Cat #237213).

2.2.1. Molecular analyses

RNA was extracted from the cultured macrophages using the RNeasy Micro Kit (Qiagen, Cat #74004) and quantified with a NanoDrop. A range of 30-100 ng of RNA was then reverse transcribed into cDNA using the Applied Biosystems cDNA synthesis kit (Cat# 4368813). The PCR reaction was performed in a 10 μL volume containing 1 μL of cDNA, 0.5 μL of each 10 μM primer, and 5 μL of 2X Applied Biosystems Power SYBR Green PCR Mastermix (ThermoFisher Scientific), with nuclease-free water. PCR was carried out using the CFX384 Touch Real-Time PCR Detection System. Relative mRNA expression levels were calculated using the $2-\Delta\Delta CT$ method. The primer sequences are provided in Supplementary Table 1.

For Western Blot Analysis (WB), RIPA lysis buffer containing a protease inhibitor cocktail (Sigma) and phosphatase inhibitors (PhosphoSTOP, Roche) were added, and samples were then sonicated and centrifuged at 12,000 rpm for 10 min at 4°C. Total protein concentration was measured using the BCA Protein Assay Kit (Biorad). The proteins were separated on SDS-polyacrylamide gels and transferred to a PVDF membrane. After blocking, the membranes were incubated with primary antibodies overnight, and then with appropriate secondary antibodies (listed in Supplementary Table 2) for 1 h. Images were captured using a transilluminator (Chemidoc MP Imaging System, BioRad), and the blots were analyzed with the Lane and Band plugin of Image Lab software (BioRad). Data were normalized first to the loading control (GAPDH) and then to the mean of the control samples (n = 6 samples analyzed per condition and time point).

The cell culture medium was collected, centrifuged, and used for the detection of IL-18 (Cat #KRC2341, ThermoFisher) and IL-1β (Cat #BMS630, ThermoFisher) by ELISA following the manufacturer's instructions.

2.2.2. Cell metabolism analysis

The oxygen consumption rate (OCR) and the extracellular acidification rate (ECAR) were measured using a Seahorse XFp Analyzer (Agilent) with Seahorse XF Cell Mito Stress Test Kit (Agilent, cat#: 103,015-100) and a Seahorse XF Glycolytic Rate Assay Kit (Agilent, cat#: 103,344-100), respectively. Briefly, 5×10^4 cells per well were seeded in 96-well Seahorse culture miniplate following the manufacturer protocol for cell suspensions. On the day of the experiment, medium was replaced with DMEM (Agilent, Cat #103680-100) supplemented with 25 mM glucose (Gibco, Cat #17504044), 2 mM glutamine (Sigma, Cat #G7513) and 1 mM sodium pyruvate (Gibco, Cat # 11360070). Respiration was measured three times under basal conditions and then five times in response to exposure to a mixture of oligomycin (1 μM) and carbonyl cyanide-4 (trifluoromethoxy) phenylhydrazone (FCCP) (1.5 μM) stressors.

2.2.3. Immunofluorescence assays

The cultures were fixed with PFA 4% for 20 min. After washing with PBS, 0.1% PBS-Tx was added for 10 min. Then, 10% Normal Donkey Serum (NDS) in 0.1% PBS-Tw was used to block non-specific markers for 1 h, followed by treatment with primary antibodies (see Supplementary Table 2) overnight at 4°C. After three washes, incubation with secondary antibodies dissolved in the blocking solution was performed, and final washing. Slides were mounted with DAPI Fluoromount-G (SouthernBiotech, Cat #0100-20). The samples were visualized with a fluorescence microscope (Nikon ECLIPSE Ni) equipped with a digital camera (DS-Ri2). The quantification of macrophages was carried out in three random fields using ImageJ (Fiji) software.

2.3. In vivo studies

Animal experiments were performed following protocols approved by the Ethical Committee of the Universitat Autònoma de Barcelona in accordance with the European Communities Council Directive 2010/63/EU. Ten weeks old male and female (1:1) Sprague Dawley rats were used. Operations were performed under anesthesia with ketamine/xylazine (90/10 mg/kg i.p.). The sciatic nerve was surgically exposed at the midthigh and carefully freed from adherences to surrounding tissues. A thin-film device of polyimide (PI) with two parallel arms of 28 mm length, 200 μm width and 12 μm thickness was longitudinally implanted in the tibial branch of the sciatic nerve with a straight needle attached to a 10–0 loop thread (STC–6, Ethicon, San Lorenzo, PR, USA), following the design of the longitudinal intrafascicular electrode (LIFE) [6,23]. After surgery, all animals were housed under standard conditions.

The treatments to modulate the FBR against intraneural PI devices began 2 days before the implantation. MCC950 (Cat #S8930, Selleckchem) and TDV19 (synthetized for the study) were administered intraperitoneally (i.p.) once a day for 2 weeks at a concentration of 10 mg/kg/day, according to previous indications [24–26]. A control group received only vehicle injections (saline solution with 5% DMSO).

We investigated whether the devices and the systemic administration of the drugs have any detrimental effects on the functional properties of the implanted nerves. Nerve conduction studies, von Frey algesimetry test, and walking track locomotion test were performed at 2 and 8 weeks post-implantation, as described in previous reports from the same laboratory [6,12].

Subgroups of rats for each treatment were euthanized at 2 and 8 weeks for histological evaluation. The sciatic nerves were dissected, fixed in 4% PFA, cryoprotected in 30% sucrose in PB, sectioned transversally into 15 μm sections using a cryostat (Leica CM190, Leica Microsystems), and processed for immunohistochemistry. For labeling macrophages and axons, sections were incubated with primary antibodies against ionized calcium binding adaptor molecule 1 (Iba1) and for neurofilament 200 kDa clone RT97, respectively, and then with Alexa-Fluor conjugated secondary antibody. The number of Iba1-positive cells in the whole tibial nerve cross-section was quantified using a custom macro for ImageJ software. The mean capsule thickness was calculated by dividing the area of the capsule surrounding the implant by the implant length in the transverse section. Given that each implant has two arms, the overall capsule thickness for each implant was determined as the average of both arms [12].

Other segments of the implanted nerves were initially fixed in 3% glutaraldehyde and 3% PFA, followed by post-fixation in 2% OsO_4, dehydration and embedding in epon resin. Thin sections of 0.5 μm were obtained using an ultramicrotome and subsequently stained with toluidine blue. To label the deposited collagen, Masson trichome staining was also performed in other nerve cross-sections according to standard protocols. In both cases, the fibrotic area around the implanted device was measured, to analyze the encapsulating tissue at different time points; using ImageJ software.

To further investigate potential the toxicological profile of the compound, another group of rats received daily i. p. Injections of TDV19 at 10 mg/kg/day, and a control group received vehicle. After 2 weeks, blood samples were taken for analysis, and samples of liver, kidney, spleen and duodenum were processed for conventional histopathological evaluation. The harvested samples were analyzed by the accredited Service of Animal Research (SIAL) of the Universitat Autònoma de Barcelona.

2.4. Data analysis

Data from in vitro and in vivo experiments are presented as mean ± SD. Statistical comparisons were made using appropriate tests, either two-way ANOVA followed by Bonferroni post-hoc test for normally distributed data, or Kruskal-Wallis test for non-normally distributed data. Test used and sample size are indicated in the figure captions. Differences were considered significant when $p < 0.05$. GraphPad Prism 8 software was used for statistics and graphics.

3. Results

3.1. Synthesis of N-((1,2,3,5,6,7-hexahydro-s-indacen-4-yl)carbamoyl)-4-(hydroxymethyl) furan-2-sulfonamide (TDV19)

Since the tertiary alcohol of MCC950 exhibits limited chemical reactivity, its direct use for surface functionalization is not optimal. Therefore, the design rationale for the compound N-((1,2,3,5,6,7-hexahydro-s-indacen-4-yl)carbamoyl)-4 (hydroxymethyl)furan-2-sulfonamide, referred as TDV19, was to preserve the core structural framework of the reference molecule, while selectively modifying the hydroxyl-bearing moiety (Fig. 1). This modification yields an analogue featuring a more reactive primary alcohol, which can serve as a chemical handle to enable covalent anchoring onto polymeric or other biomaterial surfaces.

Fig. 2 shows the synthetic pathway to obtain TDV19 (**1**). The multistep synthetic route starts from commercially available precursor ethyl furan-3-carboxylate (**2**). In the first step (**a**), compound **2** undergoes chlorosulfonylation to form the corresponding intermediate **3** [27]. Step (**b**) involves the conversion of the chlorosulfonyl derivative **3** into the corresponding amide **4**, by reaction with saturated ammonium bicarbonate solution [27]. Subsequently, in step (**c**), a reduction of the carbonyl moiety of the ester **2** yielded 4-(hydroxymethyl)furan-2-sulfonamide **5**. The reduction of the carbonyl group (**4**) to the primary alcohol (**5**) is carried out using $LiAlH_4$. Step (**d**) involves the conversion of the sulfonamide **5** in the corresponding sulfonyl azide [28], via diazotranfer imidazole-1-sulphonyl azide hydrogen sulfate salt, previously synthesized following a described procedure [29] and resulting in 4-(hydroxymethyl)furan-2-sulfonyl azide (**6**). In the last step (**e**) compound **6** reacts with 1,2,3,5,6,7-hexahydro-s-indacen-4-amine, to yield the corresponding sulfonylurea target compound **1** (TDV19) [30].

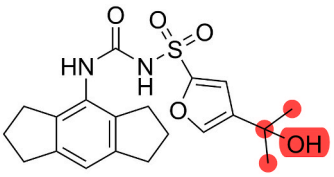

MCC950

N-((1,2,3,5,6,7-hexahydro-*s*-indacen-4-yl)carbamoyl)-4-(2-hydroxypropan-2-yl)furan-2-sulfonamide

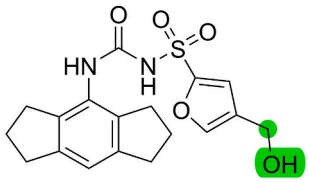

TDV19

N-((1,2,3,5,6,7-hexahydro-*s*-indacen-4-yl)carbamoyl)-4-(hydroxymethyl)furan-2-sulfonamide

Fig. 1. Chemical structure of MCC950 and TDV19, with tertiary and primary alcohol respectively.

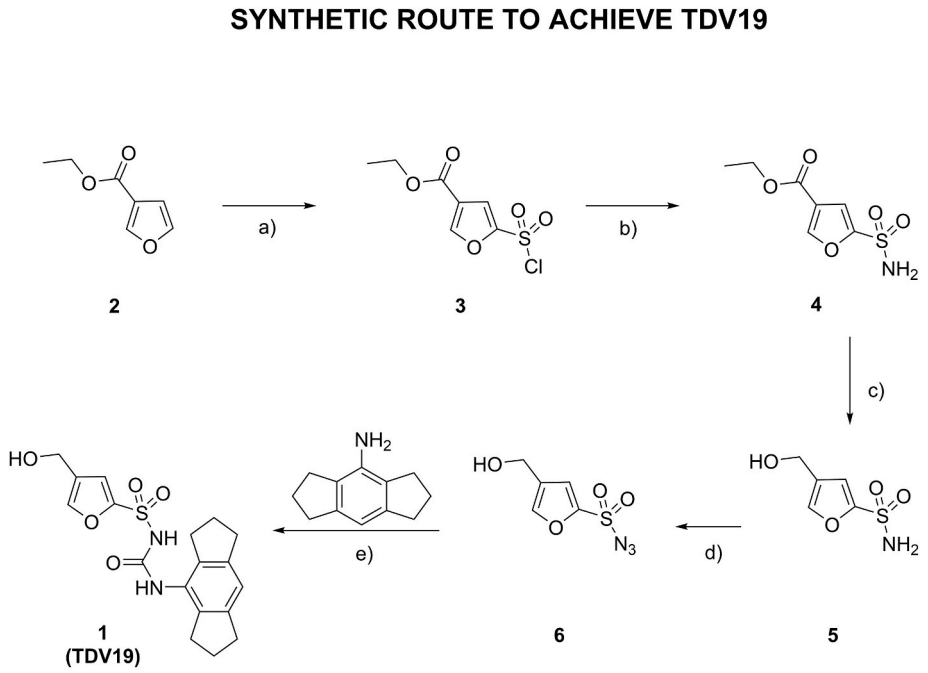

Fig. 2. Synthetic pathway to achieve TDV19 (compound 1). Reagents and conditions: (**a**) i: HSO_3Cl, DCM dry, −10°C, 72h; ii: pyridine, PCl_5, -10°C, overnight, 77%; (**b**) NH_4CO_3, water/acetone, rt, overnight, 53%; (**c**) $LiAlH_4$, THF dry, 60°C, 2h, 87%; (**d**) K_2CO_3, imidazole-1-sulphonyl azide hydrogen sulfate salt, H_2O/*i*-PrOH, rt, overnight, 58%; (**e**) $Pd(OAc)_2$, ACN dry, CO atmosphere, rt, overnight, 50%.

Additional information on the ^{1}H, ^{13}C and DEPT NMR spectra for the synthetized compounds **3**, **4**, **5**, **6** and **1** is shown in Supplementary Figs. S1–S5. Similarly, the ATR-FTIR spectra of compounds **6** and **1** can be found in Supplementary Figs. S6 and S7, whereas the HPLC spectrum of compound **1** (TDV19) is shown in Fig. S8.

3.2. *In vitro results*

We then evaluated whether the compound TDV19 exerts an inhibitory effect comparable to that of MCC950, a reference inhibitor of the NLRP3 inflammasome, by first using cultures of BMDM activated by addition of LPS. BMDMs were differentiated in culture in the presence of M-CSF and subsequently exposed to TDV19 or MCC950 and LPS. At the end of the culture period, clear morphological differences were evident among the experimental conditions (Fig. 3). In the control group, cells exhibited a predominantly elongated and spindle-shaped morphology, characterized by fine and extended cytoplasmic projections. This phenotype is consistent with macrophages in a homeostatic or alternatively activated state, typically associated with enhanced adhesion capacity and structural organization. Upon LPS stimulation, macrophages displayed a broader distribution across the culture surface, and acquired a more pronounced spindle-like morphology with prominent cytoplasmic extensions, features indicative of an activated, pro-inflammatory phenotype.

In contrast, macrophages treated with MCC950 or TDV19, in presence of LPS, showed a more rounded morphology, with clear reduction in the number and length of cytoplasmic projections. These morphological observations indicate that both MCC950 and TDV19 attenuate the structural changes triggered by LPS, promoting a phenotype more closely resembling that of non-stimulated macrophages. Similar morphological trends, such as reduced cytoplasmic spreading and restoration of a homeostatic shape, have been reported in BMDMs exposed to pharmacological modulators of inflammatory signaling [31, 32].

3.2.1. *TDV19 and MCC950 similarly modulate the activation of the NLRP3 inflammasome*

qPCR analysis revealed that LPS stimulation significantly increased the expression of mRNA levels of *NLRP3, caspase-1, IL-1β*, and *IL-18* genes compared with the control samples (Fig. 4A). Co-incubation

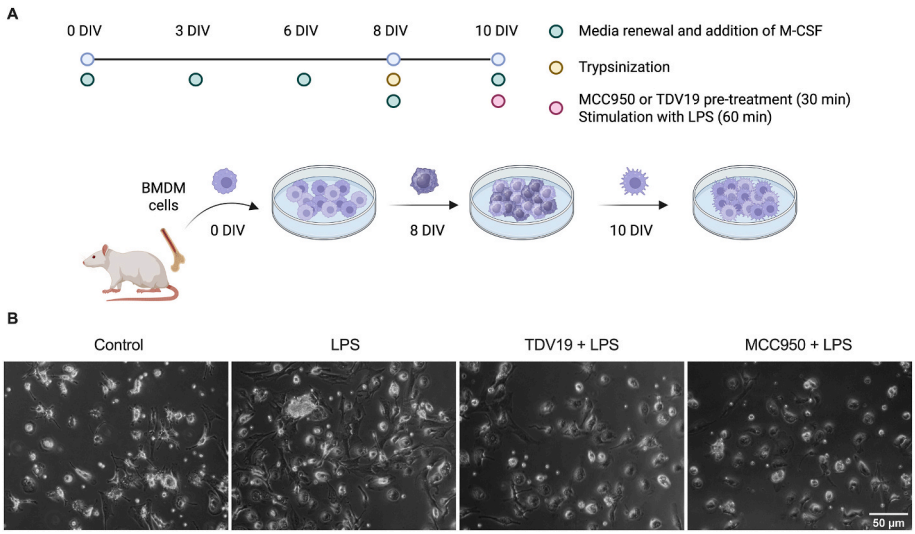

Fig. 3. Morphological changes in BMDMs following LPS stimulation and treatments with TDV19 and MCC950. **(A)** Schematic overview of the development of the in vitro experimental model and treatment protocol. DIV: days in vitro. **(B)** Phase-contrast micrographs show that control cells differentiated with M-CSF display an elongated, spindle-shaped morphology with extended cytoplasmic projections. Upon LPS stimulation (10 µg/mL, 60 min), macrophages exhibit increased spreading and larger cytoplasmic extensions, indicative of an activated phenotype. Treatments with TDV19 + LPS or MCC950 + LPS markedly reduce these structural changes, resulting in more rounded cells with fewer and shorter projections, resembling the morphology of non-stimulated macrophages. Scale bar = 50 µm.

with either TDV19 or MCC950 consistently prevented these increases, maintaining transcriptional levels close to the control values, without differences between the two compounds. Consistently, Western blot analysis revealed that the presence of TDV19 or MCC950 together with LPS markedly reduced caspase-1 and cleaved caspase-1 levels compared with LPS alone (Fig. 4B). ELISA results further confirmed that LPS clearly increased IL-1β and IL-18 release from the BMDM, whereas addition of both compounds substantially reduced their levels (Fig. 4C). Moreover, TDV19 also significantly reduced secretion of IL-1β under LPS + ATP activation of BMDM (Fig. 4D). Overall, these results indicate that TDV19 consistently reproduces the inhibitory profile of MCC950 on NLRP3 inflammasome activation and the release of associated cytokines, suggesting its potential as a therapeutic alternative in diseases driven by this inflammatory pathway.

The IC50 values for inhibiting IL-1β release in BMDM cells stimulated by LPS was calculated as 7.6 nM. This value is comparable to that of MCC950 and other inflammasome inhibitors [33].

3.2.2. *TDV19 and MCC950 similarly modulate the inflammatory profile in LPS-stimulated BMDMs*

We further investigated the inflammatory profile of the BMDMs cells in presence the LPS and both inflammasome inhibitors. LPS treatment resulted in a significant increase in both the expression of *iNos* and the release of NO to the culture medium. This effect was mitigated in the presence of MCC950 or TDV19, indicating that both compounds effectively reduce the pro-inflammatory phenotype induced by LPS (Fig. 5A).

Regarding the TNF-α cytokine, whose gene expression levels increase rapidly within the first 30-60 min post LPS stimulation [34,35], a significant increase in expression was observed following LPS treatment compared to control, whereas co-incubation with MCC950 or TDV19 resulted in a significant reduction in *Tnf-α* mRNA levels.

As for the anti-inflammatory cytokine TGF-β, LPS exposure induced a significant increase in mRNA levels relative to the control, but this increase was not observed when MCC950 or TDV19 were added to the culture. Although TGF-β is typically considered a late-expressed cytokine, our findings are consistent with recent studies suggesting that its early expression can be triggered by transcription factors such as NF-κB or AP-1 [36].

We also examined the expression of two classical markers of pro-inflammatory and anti-inflammatory macrophages, namely iNOS and CD206, respectively. LPS exposure led to a notable increase in the number of iNOS + cells, but this increase was significantly reduced when macrophages were treated with MCC950 or TDV19. Conversely, the number of CD206+ cells decreased upon LPS stimulation, but was substantially maintained when the compounds were present in the culture medium (Fig. 5B and C). Collectively, these results demonstrate that LPS treatment induces a strong pro-inflammatory response in macrophages, whereas treatment with MCC950 or with TDV19 markedly reduces this response, indicating an effective immunomodulatory action of these compounds. Interestingly, we did not find any significant difference between the two inflammasome inhibitors.

3.2.3. *TDV19 and MCC950 modulate mitochondrial metabolism in LPS-activated macrophages*

To assess whether the compounds TDV19 and MCC950 could influence the metabolic shift induced by LPS in the BMDM, mitochondrial respiration was evaluated by measuring the oxygen consumption rate (OCR), while extracellular acidification rate (ECAR) was used as an indirect indicator of glycolytic activity.

Under basal conditions, no significant differences in OCR were detected between the four experimental conditions (Fig. 6A). Following the addition of oligomycin (≈20.75 min), an inhibitor of complex V of the mitochondrial ATP synthase, OCR slightly decreased. Subsequent FCCP injection led to a significant increase in OCR in all conditions ($p < 0.0001$), reflecting enhanced maximal respiratory capacity. At this stage, significant differences were observed between control and LPS-treated macrophages ($p < 0.001$), as well as between both drug-treated groups and the LPS condition ($p < 0.05$). Finally, the combined addition of rotenone and antimycin A completely abolished mitochondrial respiration, reducing OCR to minimal levels in all conditions.

Regarding ECAR (Fig. 6B), BMDMs exposed to TDV19 or MCC950 in the presence of LPS exhibited lower values compared with both the control ($p < 0.0001$) and the LPS alone condition ($p < 0.05$). Upon oligomycin injection, ECAR values increased in all groups, with a more pronounced rise in the LPS condition, which showed significant differences compared with the other treatments. Similarly, after FCCP addition, differences among groups persisted. The subsequent addition of Rot/AA caused a significant reduction in ECAR ($p < 0.05$), except in the control condition.

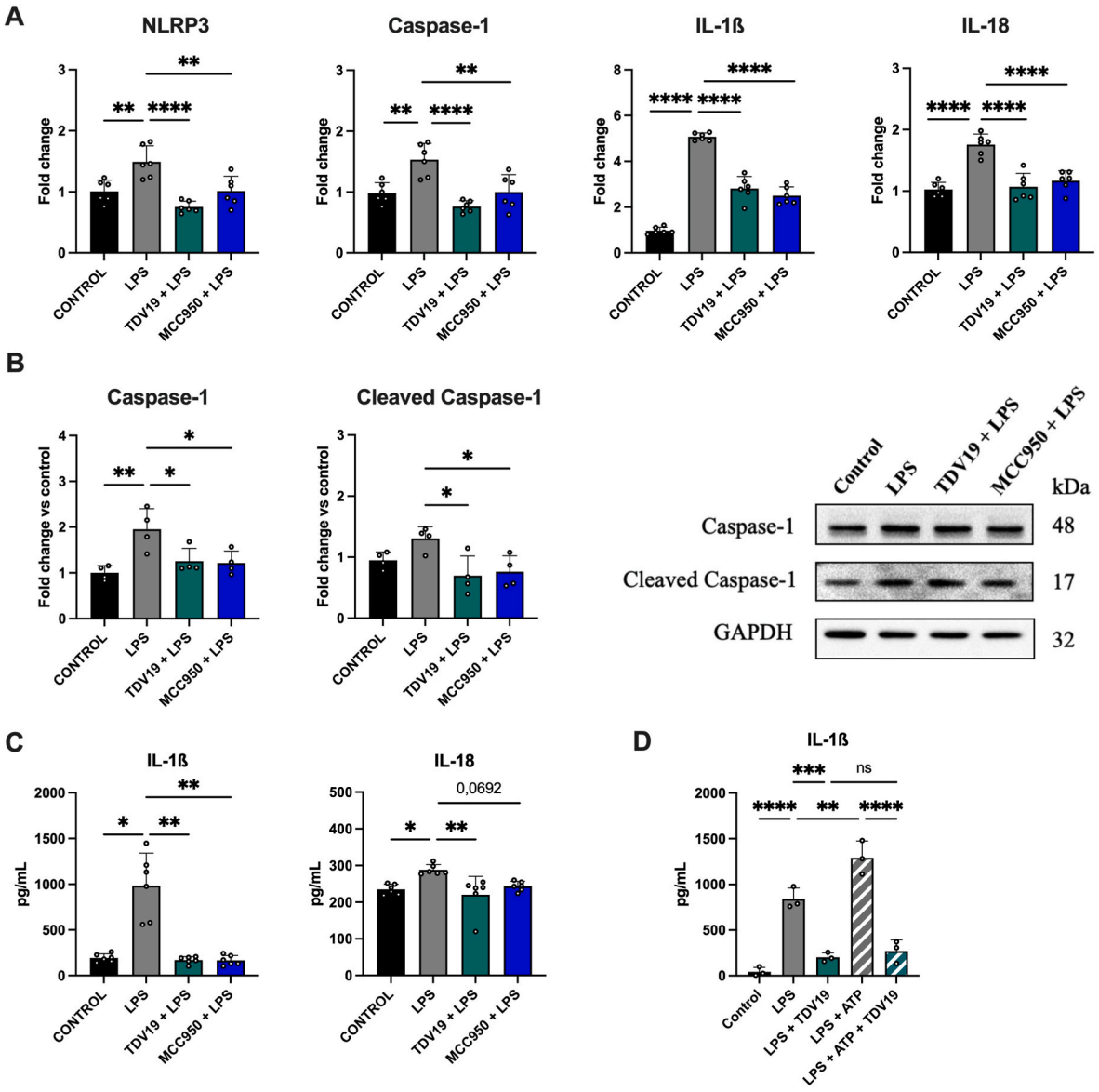

Fig. 4. TDV19 inhibits the NLRP3 inflammasome in BMDM culture. **(A)** mRNA expression of components of the NLRP3 inflammasome: NLRP3, Caspase-1, IL-1β, and IL-18. **(B)** Protein expression of Caspase-1 and Cleaved caspase-1 detected by Western blotting. **(C)** Levels of IL-1β and IL-18 in the supernatant of BMDM determined by ELISA kits. N = 4-6 cultures/condition. **(D)** Comparison of IL-1β levels in the supernatant of BMDM treated with LPS followed by ATP versus LPS alone. N = 3-4 cultures/condition. Statistical analyses by One-way ANOVA (A, C, D) and Kruskal-Wallis test (B). *p < 0.05, **p < 0.01, ***p < 0.001, ****p < 0.0001 vs. LPS. Data are presented as mean ± SD.

Finally, ATP production (Fig. 6C), calculated as the difference between the last OCR value measured before and the minimum after oligomycin injection, was reduced in LPS-treated macrophages compared to controls. Notably, ATP production was restored in both TDV19 + LPS and MCC950 + LPS conditions to values comparable to those of the control condition. Taken together, these results indicate that both TDV19 and MCC950 mitigate the LPS-induced metabolic alterations in BMDMs, partially restoring mitochondrial function and ATP production, while reducing the glycolytic shift associated with macrophage activation.

3.3. In vivo results

3.3.1. Inflammasome inhibitors do not cause alterations in peripheral nerve functions

Once demonstrated the capacity of TDV19, as well as MCC950, to reverse the pro-inflammatory phenotype of macrophages in vitro, we aimed to study the possible effect of these drugs reducing the FBR in our model of intraneural PI device implants in the rat. As demonstrated in previous studies in our laboratory [6,12], longitudinal PI implants in the sciatic nerve did not have a functional impact during the follow up to 8 weeks post-implantation. When comparing the implanted limbs with the contralateral limbs, no alterations in sensory algesimetry test, in locomotion walking track test or in nerve conduction tests were observed (Supplementary Fig. S9) following the implantation of passive PI devices. The systemic drug administration of TDV19 or MCC950 did not influence the outcomes.

3.3.2. TDV19 and MCC950 attenuate the inflammatory response and capsule formation on intraneural implants

In the early stages of the FBR, there is an intense inflammatory response characterized by the recruitment of inflammatory cells to the implantation site, as observed at 2 weeks after implantation of the PI device in the nerves (Fig. 7A). Administration of MCC950 and TDV19

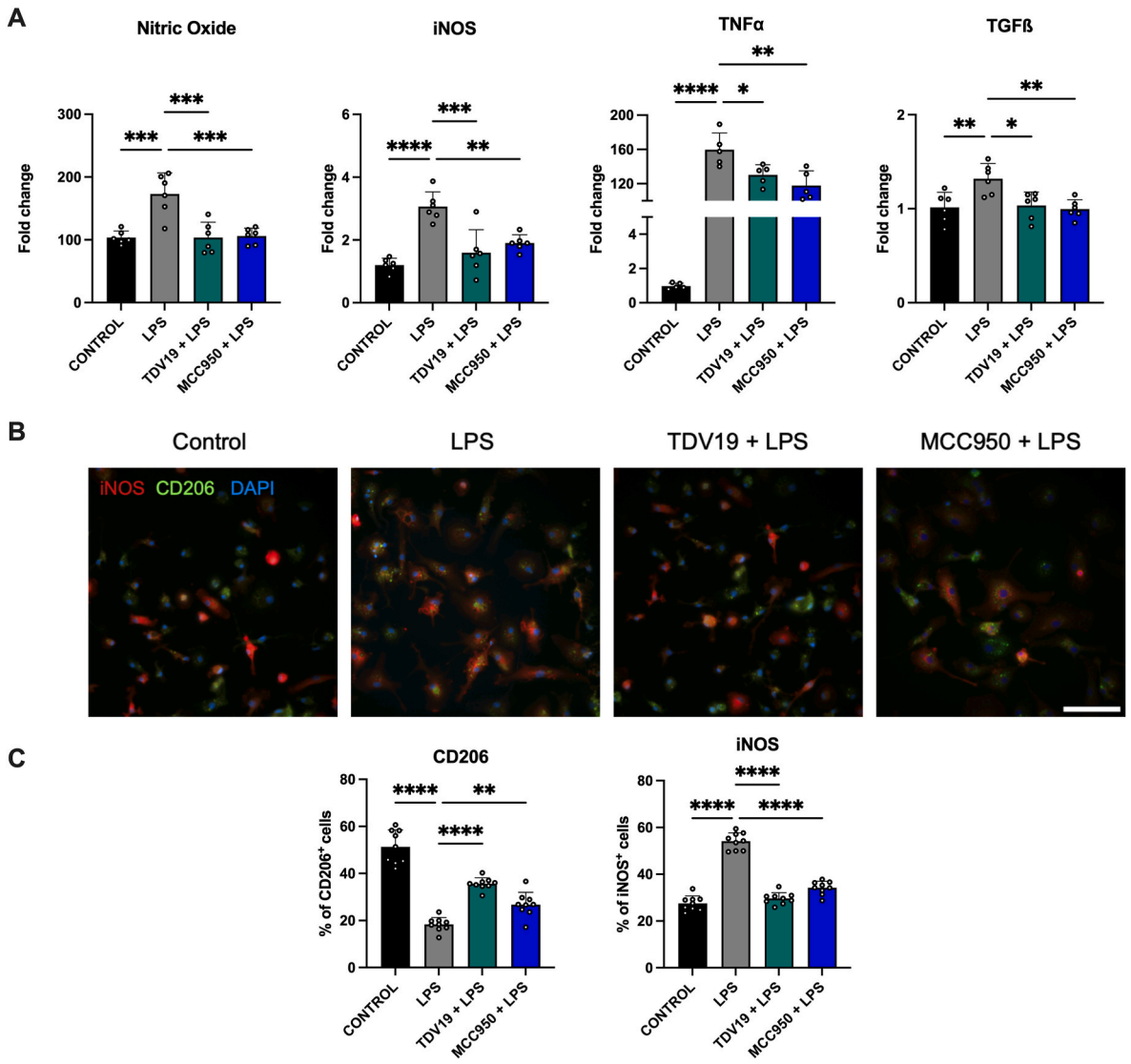

Fig. 5. Evaluation of inflammatory profile in BMDM culture. **(A)** Production of NO and mRNA expression of iNOS, TNFα and TGFβ. **(B)** Representative images of BMDM immunolabeled against iNOS (red) and CD206 (green). Dapi (blue) was applied to label nuclei. Scale bar: 100 μm. **(C)** Quantification of iNOS+ and CD206+ cells in the BMDM culture. N = 6-9 cultures/condition. Statistical analyses by Kruskal-Wallis test (A) or One-way ANOVA (C). *$p < 0.05$, **$p < 0.01$, ***$p < 0.001$, ****$p < 0.0001$ vs. LPS. Data are presented as mean ± SD.

significantly reduced macrophages infiltration compared to the control untreated group. Over time, inflammation declined in all experimental conditions, and at 8 weeks the number of IBA1+ cells was lower than at 2 weeks in the three groups ($p < 0.01$), without significant differences between them (Fig. 7B).

Correspondingly, animals treated with MCC950 and TDV19 exhibited a significant reduction of the capsule thickness at 2 and also at 8 weeks compared to controls (Fig. 7C). At 2 weeks, the capsule was predominantly composed of infiltrating inflammatory cells, as previously reported [12], and shown by Masson's trichrome staining (Fig. 8A), in which pink-stained regions correspond to inflammatory cells. By 8 weeks, fibroblasts became more prominent, and their collagen secretion (blue stain in Fig. 8A) led to the development of a fibrotic capsule isolating the implant from the surrounding tissue. The capsule became more compact, indicating a shift from an acute inflammatory phase to a collagen-rich fibrotic stage. These morphological differences are clearly visible in the images of Figs. 7A and 8A, where the treated groups exhibit a thinner, less cellular, and more organized capsule structure.

The quantitative analysis revealed that both TDV19 and MCC950 treated animals had a significant reduction in the fibrotic capsule area, compared to the control implanted group, more marked at 8 than at 2 weeks (Fig. 7C). Complementary assessment under light microscopy yielded consistent results (Fig. 8B–D). At 2 weeks, a trend toward reduced capsule formation was observed in treated groups, while at 8 weeks, the differences with respect to controls were consistently significant.

Altogether, the evaluation using three different morphological methods (immunofluorescence, Masson's trichrome staining, and light microscopy of thin sections) confirms that both TDV19 and MCC950 effectively modulate the FBR, reducing macrophage infiltration during the first phase and the fibrotic capsule formation around the intraneural PI implant.

3.3.3. *TDV19 does not induce toxicity in vivo*

We evaluated the possible toxicity generated by TDV19 compound in rats. Throughout the administration period of 2 weeks, body weight remained stable in the treated and the vehicle groups. Plasma biochemical and hematological parameters were within the normal range [37]. Particularly, the levels of key liver injury markers alanine

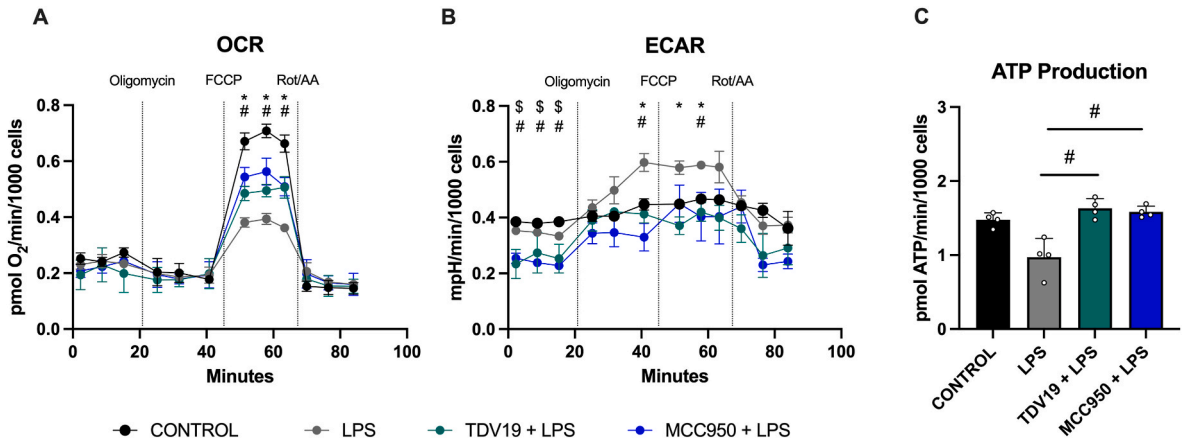

Fig. 6. TDV19 and MCC950 preserve mitochondrial respiration and ATP production while preventing LPS-induced glycolytic activation in BMDMs. **(A)** Oxygen consumption rate (OCR) and **(B)** extracellular acidification rate (ECAR) in the different experimental conditions at baseline and after sequential injection of mitochondrial electron transport chain inhibitors (oligomycin and rotenone/antimycin A [Rot/AA]) and the mitochondrial uncoupling agent FCCP. OCR and ECAR were measured three times at baseline and after each injection. Values were normalized to 1000 cells. **(C)** Total ATP production rate under each condition. N = 4 cultures/condition. Statistical analyses performed using repeated measures two-way ANOVA, mixed-effects (in A and B) followed by post hoc Bonferroni correction, and by Kruskal-Wallis test (C), followed by post hoc Dunn's correction: *p < 0.05 control vs LPS; #p < 0.05 TDV19 + LPS and MCC950 + LPS vs LPS; $ p < 0.05 TDV19 + LPS and MCC950 + LPS vs control. Data are shown as mean ± SEM.

aminotransferase (ALT) averaged 55.4 U/L and 51.2 U/L, and aspartate aminotransferase (AST) 90.7 U/L and 109.8 U/L for treated and vehicle rats respectively. No abnormalities compared to controls were observed in the histopathological examination of different organs attributable to TDV19 toxicity (see Supplementary Fig. S10).

4. Discussion

The implantation of medical devices aims to restore the shape and/or function of specific structures within the human body. The long-term survival and functionality of such implants largely depend on preventing an exaggerated foreign body reaction (FBR), a process involving inflammation, immune activation and fibrosis, culminating in the formation of a fibrotic capsule around the implant. This capsule can lead to complications, functional failure, and even progressive degradation of the biomaterial [38,39]. In the specific case of intraneural implants, aimed to serve as interfaces between the axons and external devices, such as prostheses or stimulators, one of the main consequences of the FBR is the reduction in signal recording quality and the increase in electrode impedance, ultimately shortening the useful lifespan of the device [9,40,41].

Within the field of neural interfaces, several strategies based on pharmacological modulation of the FBR have emerged, through either systemic administration or local drug release from the device surface itself. Among the compounds investigated are immunomodulatory drugs, anti-inflammatory molecules, and RGD peptides [6,11,12,20]. In this context, we have evaluated the effects of the well-known NLRP3 inhibitor MCC950 and also its analogue, TDV19, designed to improve the surface binding properties of MCC950. The choice of NLRP3 inhibitory compounds is supported by several studies in organs such as the liver, lung, kidney, and heart, where NLRP3 inhibition has been shown to reduce fibrosis and attenuate pathological processes associated with chronic inflammation [42–48]. These previous findings therefore support the rationale for designing new compounds capable of inhibiting NLRP3 inflammasome activity while minimizing adverse effects associated with MCC950, particularly renal effects [49]. This is the case for TDV19 that did not show toxic effects in our preclinical testing. Indeed, TDV19 was chemically designed to allow its immobilization onto the surface of intraneural polymeric implants, similarly to what we recently reported for dexamethasone [50]. Such local drug release would modulate the FBR while minimizing systemic side effects, as is the case for glucocorticoids [38]. The structural modification was restricted to the tertiary hydroxyl functionality, which is chemically less reactive and potentially more susceptible to dehydration under acidic conditions, such as those typically found in inflamed tissues. Moreover, the introduction of a primary alcohol enhances the hydrophilicity of the compound, potentially improving its solubility profile.

Once synthetized, it was necessary to verify through in vitro assays that TDV19 has activity comparable to that of the reference compound MCC950 to inhibit the assembly of the multiprotein NLRP3 inflammasome complex. We induced a pro-inflammatory phenotype in BMDM by LPS stimulation, and proved the ability of MCC950 and TDV19 to reverse or attenuate this activation. This approach is particularly relevant given that the NLRP3 inflammasome is present in resident macrophages of the nervous system [51,52]. TDV19 effectively reproduced the action of MCC950 by reducing the expression and secretion of key components of the NLRP3 complex assembly pathway, and inducing an anti-inflammatory phenotype of the BMDM. The TDV19 IC50 was 7.6 nM in murine BMDMs, practically the same as reported for MCC950, considered as the most potent and selective NLRP3 inhibitor to date, and similar or lower than other described inflammasome inhibitors [33].

Several studies have reported that, in vitro, exposure of macrophages to LPS induces alterations in cellular energy metabolism [53–55], that can be reversed by the addition of compounds with immunomodulatory properties [56,57]. Previous studies demonstrated that inhibition of NLRP3 via MCC950 or Coenzyme Q0 significantly modulated macrophage metabolic activity [58,59]. Consistent with these findings, our results show that TDV19 partially mitigates the effect of LPS on OCR and reduces ECAR, while total ATP production remains unaffected. These data indicate that although TDV19 modulates LPS-induced metabolic changes, it does not compromise basal mitochondrial function, supporting its potential as a safe NLRP3 inhibitor.

In our in vivo model to assess the FBR to intraneural implants, systemic administration of both MCC950 and TDV19 during the first 2 weeks not only reduced macrophage infiltration at early stages but also decreased the thickness of the fibrotic capsule at later stages of the FBR. These findings were confirmed by different histological analyses, providing strong support for the antifibrotic effect of NLRP3 inhibition in an intraneural implant model, similar to what has been shown in extraneural regenerative channels [20]. It is worth to note that daily administration of the compounds did not produce any noticeable effects on the general health status of the rats nor on the nerve function.

The mechanisms by which the inflammasome inhibitors were able to reduce the fibrotic capsule may be first explained by their effect

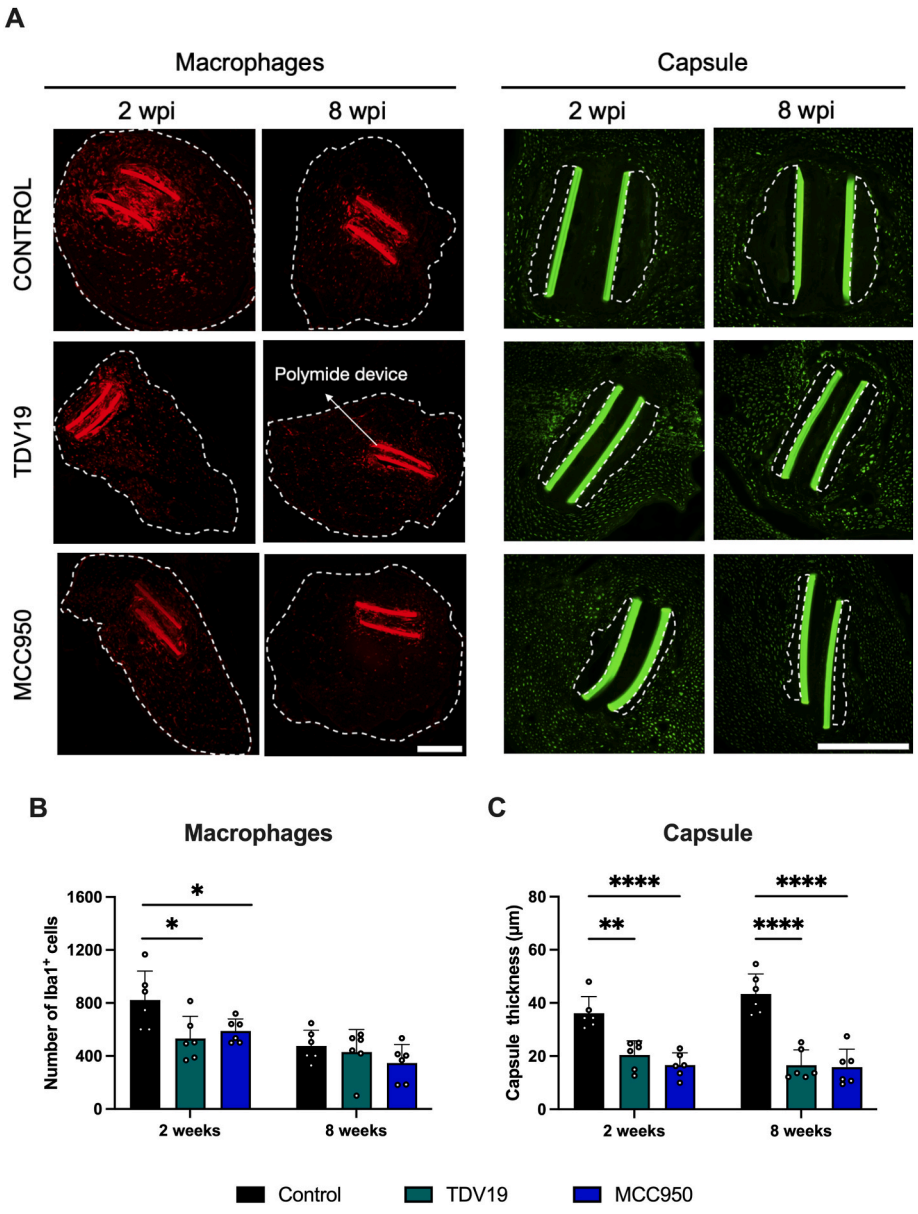

Fig. 7. FBR to intraneural PI implants. **(A)** Representative micrographs of transverse nerve sections immunolabeled against Iba1 (red) and neurofilaments (green) at 2 and 8 weeks post-implantation (2 wpi and 8 wpi) of PI devices in the three groups studied. Note the intense fluorescence emitted by the PI strips. Scale bars: 100 µm. **(B)** Histogram of the number of inflammatory Iba1+ cells in the tibial nerve (delimited by a dotted line in the microphotographs), and **(C)** Histogram of the capsule thickness (dotted line in the capsule microphotographs) around the devices in the tibial nerve of animals implanted with longitudinal PI receiving the different treatments. N = 6 animals/group. Statistical analyses using Two-way ANOVA followed by Bonferroni post-hoc test: *p < 0.05, **p < 0.01 and ****p < 0.0001. Data are presented as the mean ± SD.

reducing recruitment and activation of the macrophages in the implanted tissue. Activated macrophages secrete a variety of cytokines that collectively attract the migration of fibroblasts that, during the second phase, deposit collagen and extracellular matrix around the implant [6,60]. Thus, by modulating the initial inflammatory phase, the second fibrotic phase was also reduced. Nevertheless, a direct action of the inflammasome inhibitors on the fibroblast response cannot be excluded. In other tissues, including lungs, bowels and skin, activation of the NLRP3 inflammasome was shown to promote a profibrotic phenotype of the present fibroblasts, increasing collagen production and tissue fibrosis [61–63]. Fibroblasts present in the endoneurium and perineurium of the peripheral nerves are characterized by the expression of NGF receptors (p75NTR) [64]. Although it has not been investigated yet whether NGFR + fibroblasts express or activate the NLRP3 inflammasome, there is evidence linking neurotrophic signaling with inflammasome pathways [65]. Complementarily, in a sciatic nerve crush injury model [66] it was observed that the expression of p75NTR closely correlated with NLRP3, suggesting that this inflammasome may modulate p75NTR expression and function during nerve injuries.

5. Conclusion

Our in vitro and in vivo findings indicate that systemic administration of selective NLRP3 inhibitors significantly reduce macrophage activation and the neural FBR, supporting the hypothesis that this inflammasome plays an important role in the fibrotic response to device implants. The MCC950 analogue TDV19 was designed to retain the anti-inflammatory efficacy of MCC950, while offering additional structural versatility. In particular, the chemical features of TDV19 may facilitate its localized release from coatings or polymeric matrices, thereby

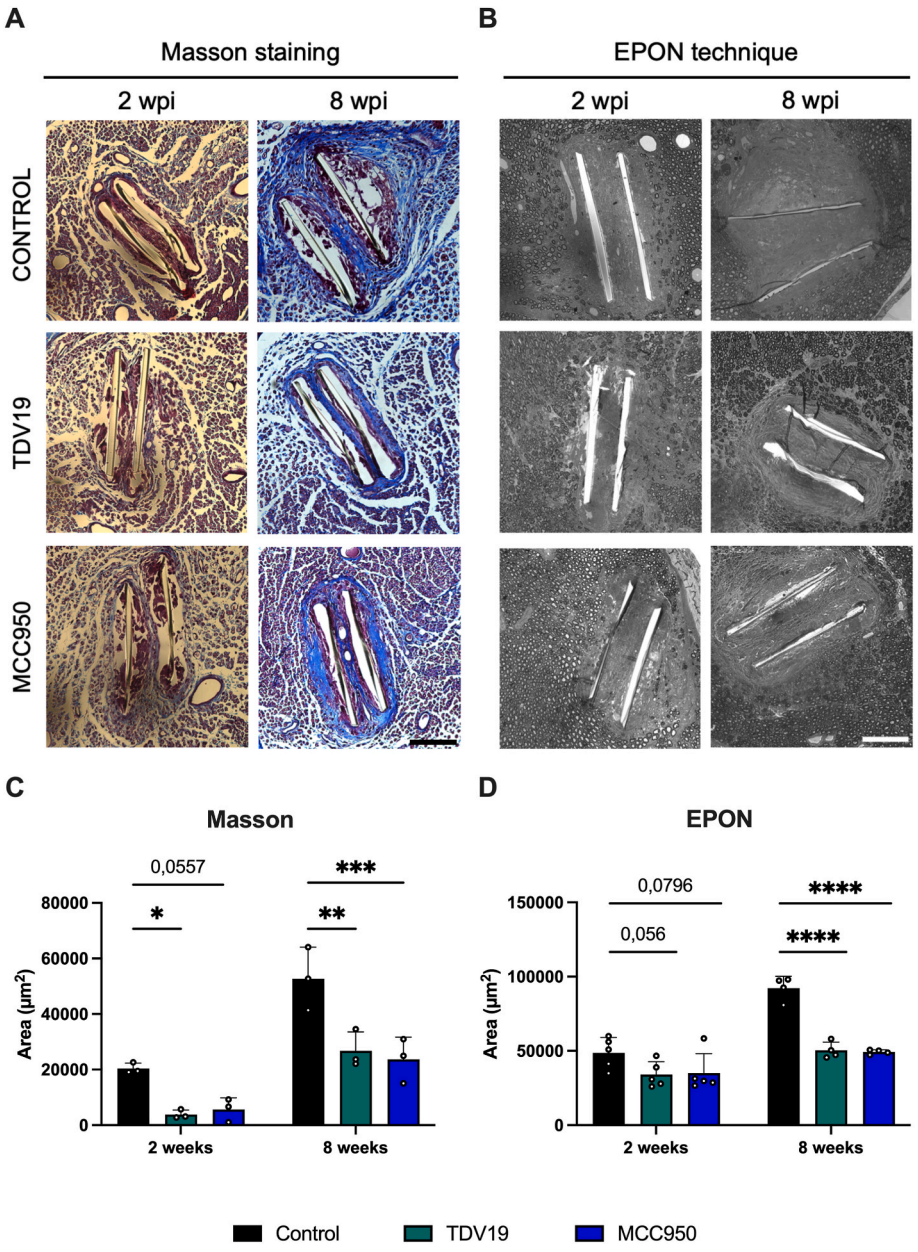

Fig. 8. Histological evaluation of the tissue response surrounding PI intraneural implants. **(A)** Representative sections stained with Masson's trichrome showing collagen deposition in the capsule surrounding the implant. At 2 weeks, the pink-stained regions indicate macrophage accumulation, while at 8 weeks, the blue-stained areas representing collagen fibers became more prominent around the device. **(B)** Representative cross-sectional images of nerves embedded in Epon resin and stained with toluidine blue, converted to grayscale, showing the microstructural organization at 2 and 8 weeks in the three study groups. Scale bars: 100 µm. **(C and D)** Histograms showing the quantification of the area surrounding the implant measured using Masson's trichrome **(C)** and light microscopy **(D)**. N = 3-6 animals/group. Statistical analyses using Two-way ANOVA followed by Bonferroni post-hoc test: *$p < 0.05$, **$p < 0.01$ ***$p < 0.001$ and ****$p < 0.0001$. Data are presented as the mean ± SD.

providing more precise control over the inflammatory microenvironment surrounding the implant. These features confer an added value compared with previously known inhibitors, positioning TDV19 as an innovative compound to enhance the long-term biocompatibility and functionality of neural electrodes.

CRediT authorship contribution statement

Jose Crugeiras: Formal analysis, Investigation, Writing – original draft. **Chiara Bisquoli:** Formal analysis, Investigation, Methodology, Writing – original draft. **María Rodríguez-Brañas:** Investigation. **Bruno Rodríguez-Meana:** Investigation, Methodology. **Tiziano De Ventura:** Investigation. **Neus Hernández:** Investigation. **Jessica Jaramillo:** Investigation. **Alice Honovich:** Investigation. **Ignacio Delgado-Martínez:** Formal analysis, Methodology. **Natalia Lago:** Conceptualization, Writing – review & editing. **Hanna Karlsson-Fernberg:** Methodology, Resources. **Maria Asplund:** Funding acquisition, Project administration, Writing – review & editing. **Stefano Carli:** Conceptualization, Supervision, Writing – review & editing. **Claudio Trapella:** Conceptualization, Supervision, Writing – original draft, Writing – review & editing. **Giulia Turrin:** Conceptualization, Investigation, Writing – original draft. **Xavier Navarro:** Conceptualization, Supervision, Writing – original draft, Writing – review & editing.

Declaration of competing interest

The authors declare that they have no known competing financial interests or personal relationships that could have appeared to influence the work reported in this paper.

Acknowledgements

This work was funded by the European Union Horizon-EIC-2022-Pathfinder Open program under grant agreement No. 101099366 (BioFINE).

The authors acknowledge the use of the Electron Microscopy Center of the University of Ferrara and the scientific and technical assistance of Dr. Cinzia Brenna and Dr. Negar Eftekhari. The RT97 antibody was obtained from the Developmental Studies Hybridoma Bank, developed under the auspices of the NICHD and maintained by the University of Iowa, Department of Biology.

Appendix A. Supplementary data

Supplementary data to this article can be found online at https://doi.org/10.1016/j.ejmcr.2026.100357.

Data availability

Data will be made available on request.

References

[1] X. Navarro, T.B. Krueger, N. Lago, S. Micera, T. Stieglitz, P. Dario, A critical review of interfaces with the peripheral nervous system for the control of neuroprostheses and hybrid bionic systems, J. Peripher. Nerv. Syst. 10 (2005) 229–258, https://doi.org/10.1111/J.1085-9489.2005.10303.X.

[2] A.B. Schwartz, X.T. Cui, D.J.J. Weber, D.W. Moran, Brain-controlled interfaces: movement restoration with neural prosthetics, Neuron 52 (2006) 205–220, https://doi.org/10.1016/J.NEURON.2006.09.019.

[3] N. Noskovicova, B. Hinz, P. Pakshir, Implant fibrosis and the underappreciated role of myofibroblasts in the foreign body reaction, Cells 10 (2021), https://doi.org/10.3390/CELLS10071794.

[4] M. Kastellorizios, N. Tipnis, D.J. Burgess, Foreign body reaction to subcutaneous implants, Adv. Exp. Med. Biol. 865 (2015) 93–108, https://doi.org/10.1007/978-3-319-18603-0_6.

[5] J.M. Anderson, A. Rodriguez, D.T. Chang, Foreign body reaction to biomaterials, Semin. Immunol. 20 (2008) 86–100, https://doi.org/10.1016/J.SMIM.2007.11.004.

[6] N. de la Oliva, X. Navarro, J. del Valle, Time course study of long-term biocompatibility and foreign body reaction to intraneural polyimide-based implants, J. Biomed. Mater. Res. 106 (2018) 746–757, https://doi.org/10.1002/JBM.A.36274.

[7] W.M. Grill, J.T. Mortimer, Neural and connective tissue response to long-term implantation of multiple contact nerve cuff electrodes, J. Biomed. Mater. Res. 50 (2000) 215–226, https://doi.org/10.1002/(sici)1097-4636(200005)50:2<215::aid-jbm17>3.0.co;2-a.

[8] F. Lotti, F. Ranieri, G. Vadalà, L. Zollo, G. Di Pino, Invasive intraneural interfaces: foreign body reaction issues, Front. Neurosci. 11 (2017), https://doi.org/10.3389/FNINS.2017.00497.

[9] S. Raspopovic, M. Capogrosso, F.M. Petrini, M. Bonizzato, J. Rigosa, G. Di Pino, J. Carpaneto, M. Controzzi, T. Boretius, E. Fernandez, G. Granata, C.M. Oddo, L. Citi, A.L. Ciancio, C. Cipriani, M.C. Carrozza, W. Jensen, E. Guglielmelli, T. Stieglitz, P.M. Rossini, S. Micera, Restoring natural sensory feedback in real-time bidirectional hand prostheses, Sci. Transl. Med. 6 (2014), https://doi.org/10.1126/SCITRANSLMED.3006820.

[10] A. Carnicer-Lombarte, S.T. Chen, G.G. Malliaras, D.G. Barone, Foreign body reaction to implanted biomaterials and its impact in nerve neuroprosthetics, Front. Bioeng. Biotechnol. 9 (2021), https://doi.org/10.3389/FBIOE.2021.622524.

[11] J.J. Fitzgerald, Suppression of scarring in peripheral nerve implants by drug elution, J. Neural. Eng. 13 (2016), https://doi.org/10.1088/1741-2560/13/2/026006.

[12] B. Rodríguez-Meana, J. del Valle, X. Navarro, A combinatory therapy of metformin and dexamethasone reduces the foreign body reaction to intraneural electrodes, Cells 13 (2024) 2112, https://doi.org/10.3390/CELLS13242112/S1.

[13] M.S.J. Mangan, E.J. Olhava, W.R. Roush, H.M. Seidel, G.D. Glick, E. Latz, Targeting the NLRP3 inflammasome in inflammatory diseases, Nat. Rev. Drug Discov. 17 (2018) 588–606, https://doi.org/10.1038/NRD.2018.97.

[14] M.R. de Zoete, N.W. Palm, S. Zhu, R.A. Flave, Inflammasomes, Cold Spring Harbor Perspect. Biol. 6 (2014) a016287, https://doi.org/10.1101/CSHPERSPECT.A016287.

[15] S.M. Man, T.D. Kanneganti, Regulation of inflammasome activation, Immunol. Rev. 265 (2015) 6–21, https://doi.org/10.1111/IMR.12296.

[16] M.J. Caballero-Herrero, E. Jumilla, M. Buitrago-Ruiz, G. Valero-Navarro, S. Cuevas, Role of damage-associated molecular patterns (DAMPS) in the postoperative period after colorectal surgery, Int. J. Mol. Sci. 24 (2023) 3862, https://doi.org/10.3390/IJMS24043862.

[17] D.G. Perregaux, P. McNiff, R. Laliberte, N. Hawryluk, H. Peurano, E. Stam, J. Eggler, R. Griffiths, M.A. Dombroski, C.A. Gabel, Identification and characterization of a novel class of interleukin-1 post-translational processing inhibitors, J. Pharmacol. Exp. Therapeut. 299 (2001) 187–197.

[18] M.J. Primiano, B.A. Lefker, M.R. Bowman, A.G. Bree, C. Hubeau, P.D. Bonin, M. Mangan, K. Dower, B.G. Monks, L. Cushing, S. Wang, J. Guzova, A. Jiao, L.-L. Lin, E. Latz, D. Hepworth, J.P. Hall, Efficacy and pharmacology of the NLRP3 inflammasome inhibitor CP-456,773 (CRID3) in murine models of dermal and pulmonary inflammation, J. Immunol. 197 (2016) 2421–2433, https://doi.org/10.4049/JIMMUNOL.1600035.

[19] R.C. Coll, A.A.B. Robertson, J.J. Chae, S.C. Higgins, R. Muñoz-Planillo, M. C. Inserra, I. Vetter, L.S. Dungan, B.G. Monks, A. Stutz, D.E. Croker, M.S. Butler, M. Haneklaus, C.E. Sutton, G. Núñez, E. Latz, D.L. Kastner, K.H.G. Mills, S. L. Masters, K. Schroder, M.A. Cooper, L.A.J. O'Neill, A small-molecule inhibitor of the NLRP3 inflammasome for the treatment of inflammatory diseases, Nat. Med. 21 (2015) 248–257, https://doi.org/10.1038/NM.3806.

[20] D.G. Barone, A. Carnicer-Lombarte, P. Tourlomousis, R.S. Hamilton, M. Prater, A. L. Rutz, I.B. Dimov, G.G. Malliaras, S.P. Lacour, A.A.B. Robertson, K. Franze, J. W. Fawcett, C.E. Bryant, Prevention of the foreign body response to implantable medical devices by inflammasome inhibition, Proc. Natl. Acad. Sci. U. S. A. 119 (2022) e2115857119, https://doi.org/10.1073/PNAS.2115857119.

[21] P. Barraja, P. Diana, A. Lauria, A. Montalbano, A.M. Almerico, G. Dattolo, G. Cirrincione, G. Viola, F. Dall'Acqua, Pyrrolo[2,3-h]quinolinones: synthesis and photochemotherapic activity, Bioorg. Med. Chem. Lett 13 (2003) 2809–2811, https://doi.org/10.1016/s0960-894x(03)00529-8.

[22] E.M. Grimsey, L.J.V. Piddock, Do phenothiazines possess antimicrobial and efflux inhibitory properties? FEMS Microbiol. Rev. 43 (2019) 577–590, https://doi.org/10.1093/femsre/fuz017. PMID: 31216574.

[23] N. Lago, K. Yoshida, K.P. Koch, X. Navarro, Assessment of biocompatibility of chronically implanted polyimide and platinum intrafascicular electrodes, IEEE Trans. Biomed. Eng. 54 (2007) 281–290, https://doi.org/10.1109/TBME.2006.886617.

[24] L. Zhang, Y.H. Jiang, C. Fan, Q. Zhang, Y.H. Jiang, Y. Li, Y.T. Xue, MCC950 attenuates doxorubicin-induced myocardial injury in vivo and in vitro by inhibiting NLRP3-mediated pyroptosis, Biomed. Pharmacother. 143 (2021), https://doi.org/10.1016/J.BIOPHA.2021.112133.

[25] J.M. Li, T. Hu, X.N. Zhou, T. Zhang, J.H. Guo, M.Y. Wang, Y.L. Wu, W.J. Su, C. L. Jiang, The involvement of NLRP3 inflammasome in CUMS-induced AD-like pathological changes and related cognitive decline in mice, J. Neuroinflammation 20 (2023), https://doi.org/10.1186/S12974-023-02791-0.

[26] I. Martínez-Martel, S.E. Negrini-Ferrari, O. Pol, MCC950 reduces the anxiodepressive-like behaviors and memory deficits related to paclitaxel-induced peripheral neuropathy in mice, Antioxidants 14 (2025), https://doi.org/10.3390/ANTIOX14020143.

[27] F.J. Urban, V.J. Jasys, J.W. Raggon, R.A. Buzon, P.D. Hill, J.F. Eggler, J.D. Weaver, Novel synthesis of 1-(1,2,3,5,6,7-Hexahydro- s-indacen-4-yl)-3-[4-(1-hydroxy-1-methyl-ethyl)-furan-2-sulfonyl]urea, an anti-inflammatory agent, Synth. Commun. 33 (2003) 2029–2043, https://doi.org/10.1081/SCC-120021029.

[28] M.Y. Stevens, R.T. Sawant, L.R. Odell, Synthesis of sulfonyl azides via diazotransfer using an imidazole-1-sulfonyl azide salt: scope and 15N NMR labeling experiments, J. Org. Chem. 79 (2014) 4826–4831, https://doi.org/10.1021/JO500553Q.

[29] G.T. Potter, G.C. Jayson, G.J. Miller, J.M. Gardiner, An updated synthesis of the diazo-transfer reagent imidazole-1-sulfonyl azide hydrogen sulfate, J. Org. Chem. 81 (2016) 3443–3446, https://doi.org/10.1021/ACS.JOC.6B00177.

[30] J. Zhao, Z. Li, S. Song, M.A. Wang, B. Fu, Z. Zhang, Product-derived bimetallic palladium complex catalyzes direct carbonylation of sulfonylazides, Angew Chem. Int. Ed. Engl. 55 (2016) 5545–5549, https://doi.org/10.1002/ANIE.201600887.

[31] S. Wang, S. Xu, J. Zhou, L. Zhang, X. Mao, X. Yao, C. Liu, Luteolin transforms the polarity of bone marrow-derived macrophages to regulate the cytokine storm, J. Inflamm. 18 (2021) 21, https://doi.org/10.1186/S12950-021-00285-5.

[32] A. Scafidi, F. Lind-Holm Mogensen, E. Campus, A. Pailas, K. Neumann, N. Legrave, F. Bernardin, S.L. Pereira, P.M.A. Antony, N. Nicot, M. Mittelbronn, A. Grünewald, P.V. Nazarov, A. Poli, E. Van Dyck, A. Michelucci, Metformin impacts the differentiation of mouse bone marrow cells into macrophages affecting tumour immunity, Heliyon 10 (2024) e37792, https://doi.org/10.1016/J.HELIYON.2024.E37792.

[33] S. El-Sayed, S. Freeman, R.A. Bryce, A selective review and virtual screening analysis of natural product inhibitors of the NLRP3 inflammasome, Molecules 27 (2022) 6213, https://doi.org/10.3390/molecules27196213.

[34] J. Xaus, M. Comalada, A.F. Valledor, J. Lloberas, F. López-Soriano, J.M. Argilés, C. Bogdan, A. Celada, LPS induces apoptosis in macrophages mostly through the autocrine production of TNF-α, Blood 95 (2000) 3823–3831, https://doi.org/10.1182/BLOOD.V95.12.3823.

[35] C.D. Dumitru, J.D. Ceci, C. Tsatsanis, D. Kontoyiannis, K. Stamatakis, J.H. Lin, C. Patriotis, N.A. Jenkins, N.G. Copeland, G. Kollias, P.N. Tsichlis, TNF-α induction by LPS is regulated posttranscriptionally via a Tpl2/ERK-dependent pathway, Cell 103 (2000) 1071–1083, https://doi.org/10.1016/S0092-8674(00)00210-5.

[36] J. Cornice, D. Verzella, P. Arboretto, D. Vecchiotti, D. Capece, F. Zazzeroni, G. Franzoso, NF-κB: governing macrophages in cancer, Genes 15 (2024) 197, https://doi.org/10.3390/GENES15020197.

[37] Q. He, G. Su, K. Liu, F. Zhang, Y. Jiang, J. Gao, L. Liu, Z. Jiang, M. Jin, H. Xie, Sex-specific reference intervals of hematologic and biochemical analytes in sprague-dawley rats using the nonparametric rank percentile method, PLoS One 12 (12) (2017) e0189837, https://doi.org/10.1371/journal.pone.0189837.
[38] N. Kalashnikov, J. Barralet, J. Vorstenbosch, Implantable medical devices, biomaterials, and the foreign body response: a surgical perspective, J. Biomed. Mater. Res. 113 (2025) e37983, https://doi.org/10.1002/JBM.A.37983.
[39] A.N. Dalrymple, S.T. Jones, J.B. Fallon, R.K. Shepherd, D.J. Weber, Overcoming failure: improving acceptance and success of implanted neural interfaces, Bioelectron. Med. 11 (2025) 6, https://doi.org/10.1186/S42234-025-00168-7.
[40] B.S. Spearman, V.H. Desai, S. Mobini, M.D. McDermott, J.B. Graham, K.J. Otto, J. W. Judy, C.E. Schmidt, Tissue-engineered peripheral nerve interfaces, Adv. Funct. Mater. 28 (2018) 1701713, https://doi.org/10.1002/ADFM.201701713.
[41] T.S. Davis, H.A.C. Wark, D.T. Hutchinson, D.J. Warren, K. O'Neill, T. Scheinblum, G.A. Clark, R.A. Normann, B. Greger, Restoring motor control and sensory feedback in people with upper extremity amputations using arrays of 96 microelectrodes implanted in the median and ulnar nerves, J. Neural. Eng. 13 (2016) 036001, https://doi.org/10.1088/1741-2560/13/3/036001.
[42] A.R. Mridha, A. Wree, A.A.B. Robertson, M.M. Yeh, C.D. Johnson, D.M. Van Rooyen, F. Haczeyni, N.C.H. Teoh, C. Savard, G.N. Ioannou, S.L. Masters, K. Schroder, M.A. Cooper, A.E. Feldstein, G.C. Farrell, NLRP3 inflammasome blockade reduces liver inflammation and fibrosis in experimental NASH in mice, J. Hepatol. 66 (2017) 1037, https://doi.org/10.1016/J.JHEP.2017.01.022.
[43] S. Wu, Q. Cheng, Y. Shi, M. Liu, K. Tan, B. Liao, Inhibition of NLRP3 inflammasome activation alleviated liver injury and wasting effect in tumor-bearing mice, Sci. Rep. 15 (2025) 39533, https://doi.org/10.1038/S41598-025-23323-1.
[44] R. Gao, H. Shi, S. Chang, Y. Gao, X. Li, C. Lv, H. Yang, H. Xiang, J. Yang, L. Xu, Y. Tang, The selective NLRP3-inflammasome inhibitor MCC950 reduces myocardial fibrosis and improves cardiac remodeling in a mouse model of myocardial infarction, Int. Immunopharmacol. 74 (2019) 105575, https://doi.org/10.1016/J.INTIMP.2019.04.022.
[45] S.M. Krishnan, Y.H. Ling, B.M. Huuskes, D.M. Ferens, N. Saini, C.T. Chan, H. Diep, M.M. Kett, C.S. Samuel, B.K. Kemp-Harper, A.A.B. Robertson, M.A. Cooper, K. Peter, E. Latz, A.S. Mansell, C.G. Sobey, G.R. Drummond, A. Vinh, Pharmacological inhibition of the NLRP3 inflammasome reduces blood pressure, renal damage, and dysfunction in salt-sensitive hypertension, Cardiovasc. Res. 115 (2018) 776, https://doi.org/10.1093/CVR/CVY252.
[46] C. Zhang, X. Zhu, L. Li, T. Ma, M. Shi, Y. Yang, Q. Fan, A small molecule inhibitor MCC950 ameliorates kidney injury in diabetic nephropathy by inhibiting NLRP3 inflammasome activation, Diabetes Metab. Syndr. Obes. 12 (2019) 1297, https://doi.org/10.2147/DMSO.S199802.
[47] M. Wang, M. Zhao, J. Yu, Y. Xu, J. Zhang, J. Liu, Z. Zheng, J. Ye, Z. Wang, D. Ye, Y. Feng, S. Xu, W. Pan, C. Wei, J. Wan, MCC950, a selective NLRP3 inhibitor, attenuates adverse cardiac remodeling following heart failure through improving the cardiometabolic dysfunction in obese mice, Front. Cardiovasc. Med. 9 (2022) 727474, https://doi.org/10.3389/FCVM.2022.727474/BIBTEX.
[48] R. Al-Qazazi, P.D.A. Lima, S.Z. Prisco, F. Potus, A. Dasgupta, K.H. Chen, L. Tian, R. E.T. Bentley, J. Mewburn, A.Y. Martin, D. Wu, O. Jones, D.H. Maurice, S. Bonnet, S. Provencher, K.W. Prins, S.L. Archer, Macrophage–NLRP3 activation promotes right ventricle failure in pulmonary arterial hypertension, Am. J. Respir. Crit. Care Med. 206 (2022) 608–624, https://doi.org/10.1164/RCCM.202110-2274OC/SUPPL_FILE/DISCLOSURES.PDF.
[49] J.A. Østergaard, J.C. Jha, A. Sharma, A. Dai, J.S.Y. Choi, J.B. De Haan, M. E. Cooper, K. Jandeleit-Dahl, Adverse renal effects of NLRP3 inflammasome inhibition by MCC950 in an interventional model of diabetic kidney disease, Clin. Sci. (Lond.) 136 (2022) 167–180, https://doi.org/10.1042/CS20210865.
[50] G. Turrin, J. Crugeiras, C. Bisquoli, D. Barboni, M. Catani, B. Rodríguez-Meana, R. Boaretto, M. Albicini, S. Caramori, C. Trapella, T. Stieglitz, Y. Baslan, H. Karlsson-Fernberg, F.L. Narvaez-Chicaiza, E. Marchini, A. Cavazzini, R. López-Vales, M. Asplund, X. Navarro, S. Carli, Covalent binding of dexamethasone to polyimide improves biocompatibility of neural implantable devices, Adv. Healthcare Mater. 14 (2025) 2405004, https://doi.org/10.1002/ADHM.202405004.
[51] G. Guarda, M. Zenger, A.S. Yazdi, K. Schroder, I. Ferrero, P. Menu, A. Tardivel, C. Mattmann, J. Tschopp, Differential expression of NLRP3 among hematopoietic cells, J. Immunol. 186 (2011) 2529–2534, https://doi.org/10.4049/JIMMUNOL.1002720.
[52] A. Gustin, M. Kirchmeyer, E. Koncina, P. Felten, S. Losciuto, T. Heurtaux, A. Tardivel, P. Heuschling, C. Dostert, NLRP3 inflammasome is expressed and functional in mouse brain microglia but not in astrocytes, PLoS One 10 (2015) e0130624, https://doi.org/10.1371/JOURNAL.PONE.0130624.
[53] V. Vijayan, P. Pradhan, L. Braud, H.R. Fuchs, F. Gueler, R. Motterlini, R. Foresti, S. Immenschuh, Human and murine macrophages exhibit differential metabolic responses to lipopolysaccharide - a divergent role for glycolysis, Redox Biol. 22 (2019) 101147, https://doi.org/10.1016/J.REDOX.2019.101147.
[54] W. Yu, X. Wang, J. Zhao, R. Liu, J. Liu, Z. Wang, J. Peng, H. Wu, X. Zhang, Z. Long, D. Kong, W. Li, C. Hai, Stat2-Drp1 mediated mitochondrial mass increase is necessary for pro-inflammatory differentiation of macrophages, Redox Biol. 37 (2020) 101761, https://doi.org/10.1016/J.REDOX.2020.101761.
[55] P. Kanmani, G. Hu, Quantification of intracellular and mitochondrial ATP content in macrophages during lipopolysaccharide-induced inflammatory response, Methods Cell Biol. 194 (2025) 77–92, https://doi.org/10.1016/BS.MCB.2024.01.006.
[56] S.T. Liao, C. Han, D.Q. Xu, X.W. Fu, J.S. Wang, L.Y. Kong, 4-Octyl itaconate inhibits aerobic glycolysis by targeting GAPDH to exert anti-inflammatory effects, Nat. Commun. 10 (2019) 1–11, https://doi.org/10.1038/s41467-019-13078-5.
[57] B. Kelly, G.M. Tannahill, M.P. Murphy, L.A.J. O'Neill, Metformin inhibits the production of reactive oxygen species from NADH:Ubiquinone oxidoreductase to limit induction of interleukin-1β (IL-1β) and boosts interleukin-10 (IL-10) in lipopolysaccharide (LPS)-activated macrophages, J. Biol. Chem. 290 (2015) 20348, https://doi.org/10.1074/JBC.M115.662114.
[58] O.M. Finucane, J. Sugrue, A. Rubio-Araiz, M.V. Guillot-Sestier, M.A. Lynch, The NLRP3 inflammasome modulates glycolysis by increasing PFKFB3 in an IL-1β-dependent manner in macrophages, Sci. Rep. 9 (2019) 4034, https://doi.org/10.1038/s41598-019-40619-1.
[59] Y.C. Hseu, Y.F. Tseng, S. Pandey, S. Shrestha, K.Y. Lin, C.W. Lin, C.C. Lee, S. T. Huang, H.L. Yang, Coenzyme Q0 inhibits NLRP3 inflammasome activation through mitophagy induction in LPS/ATP-stimulated macrophages, Oxid. Med. Cell. Longev. 2022 (2022) 4266214, https://doi.org/10.1155/2022/4266214.
[60] A. Carnicer-Lombarte, S.T. Chen, G.G. Malliaras, D.G. Barone, Foreign body reaction to implanted biomaterials and its impact in nerve neuroprosthetics, Front. Bioeng. Biotechnol. 9 (2021) 622524, https://doi.org/10.3389/FBIOE.2021.622524.
[61] T.H. Nguyen, H.H.N. Nguyen, T.D. Nguyen, V.T.H. Tran, H.A. Nguyen, D.V. Pham, NLRP3 inflammasome activation contributes to the development of the pro-fibrotic phenotype of lung fibroblasts, Biochem. Pharmacol. 229 (2024) 116496, https://doi.org/10.1016/J.BCP.2024.116496.
[62] S. Weber, S. Sitte, A.L. Voegele, L. Sologub, A. Wilfer, T. Rath, A. Nägel, S. Zundler, L. Franchi, A.W. Opipari, S. Sonnewald, S. Reid, A. Hartmann, P. Eichhorn, C. Handtrack, K. Weber, R. Grützmann, C. Neufert, V.S. Schellerer, E. Naschberger, A.B. Ekici, C. Büttner, M.F. Neurath, R. Atreya, NLRP3 inhibition leads to impaired mucosal fibroblast function in patients with inflammatory bowel diseases, J. Crohns Colitis 18 (2024) 446–461, https://doi.org/10.1093/ECCO-JCC/JJAD164.
[63] J. Zhao, S. Zhang, Z. Gong, W. Mao, W. Bao, Q. Li, Y. Bai, F. Gao, S. Feng, NLRP3: a key regulator of skin wound healing and macrophage-fibroblast interactions in mice, Cell Commun. Signal. 23 (2025) 55, https://doi.org/10.1186/S12964-025-02063-9/FIGURES/10.
[64] L. Steele, B. Olabi, K. Roberts, P. V Mazin, S. Koplev, C. Tudor, B. Rumney, C. Admane, T. Jiang, D. Correa-Gallegos, K. Priya Chakala, A. Binkevich, N. Hudaa Gopee, A. Predeus, M. Prete, E. Winheim, K. Annusver, A. Forsthuber, L. Francis, S. Frech, C. Ganier, T. Layton, Y. Liu, H. Yuan, J.E. Gudjonsson, B. M. Lichtenberger, S. Mahil, J. Nanchahal, E.A. Otoole, M. V Plikus, Y. Rinkevich, E. Rognoni, C.H. Smith, S.A. Teichmann, M. Kasper, A.R. Foster, M. Lotfollahi, M. Haniffa, A single-cell and spatial genomics atlas of human skin fibroblasts reveals shared disease-related fibroblast subtypes across tissues, Nat. Immunol. 26 (2025) 1807–1820, https://doi.org/10.1038/s41590-025-02267-8.
[65] A. Datta-Mitra, S. Kundu-Raychaudhuri, A. Mitra, S.P. Raychaudhuri, Cross talk between neuroregulatory molecule and monocyte: nerve growth factor activates the inflammasome, PLoS One 10 (2015) e0121626, https://doi.org/10.1371/JOURNAL.PONE.0121626.
[66] M. Cui, J. Liang, D. Xu, L. Zhao, X. Zhang, L. Zhang, S. Ren, D. Liu, X. Niu, Y. jin Zang, B. Zhang, NLRP3 inflammasome is involved in nerve recovery after sciatic nerve injury, Int. Immunopharmacol. 84 (2020) 106492, https://doi.org/10.1016/J.INTIMP.2020.106492.